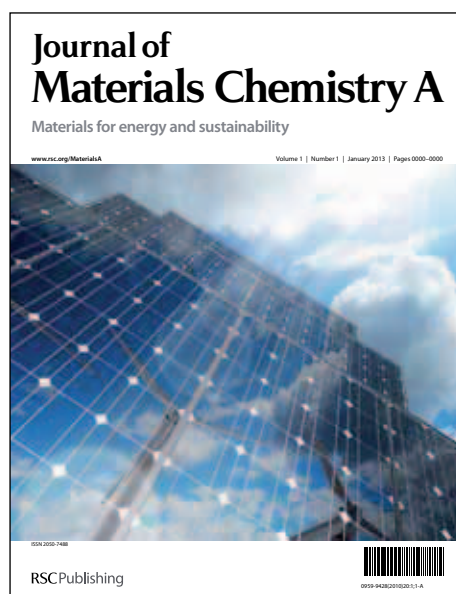


Journal of Materials Chemistry A

Accepted Manuscript



This is an *Accepted Manuscript*, which has been through the RSC Publishing peer review process and has been accepted for publication.

Accepted Manuscripts are published online shortly after acceptance, which is prior to technical editing, formatting and proof reading. This free service from RSC Publishing allows authors to make their results available to the community, in citable form, before publication of the edited article. This *Accepted Manuscript* will be replaced by the edited and formatted *Advance Article* as soon as this is available.

To cite this manuscript please use its permanent Digital Object Identifier (DOI®), which is identical for all formats of publication.

More information about *Accepted Manuscripts* can be found in the [Information for Authors](#).

Please note that technical editing may introduce minor changes to the text and/or graphics contained in the manuscript submitted by the author(s) which may alter content, and that the standard [Terms & Conditions](#) and the [ethical guidelines](#) that apply to the journal are still applicable. In no event shall the RSC be held responsible for any errors or omissions in these *Accepted Manuscript* manuscripts or any consequences arising from the use of any information contained in them.

ARTICLE

Hybrid Porous Polymers Constructed from Octavinylsilsesquioxane and Benzene via Friedel–Crafts Reaction: Tunable Porosity, Gas Sorption, and Postfunctionalization

Cite this: DOI: 10.1039/x0xx00000x

Received 00th January 2012,
Accepted 00th January 2012

DOI: 10.1039/x0xx00000x

www.rsc.org/

Yue Wu,^{a,b} Dengxu Wang,^a Liguang Li,^a Wenyang Yang,^a Shengyu Feng,^{*a} and Hongzhi Liu^{*a}

Friedel–Crafts reaction of cubic octavinylsilsesquioxane (OVS) and benzene results in a series of hybrid porous polymers (HPPs). The resulting materials, HPP-1 to HPP-4, show relatively high porosity with apparent Brunauer–Emmett–Teller surface areas in a range of 400 m² g⁻¹ to 904 m² g⁻¹, with total pore volumes in the range of 0.24 cm³ g⁻¹ to 0.99 cm³ g⁻¹. Their porosities can be fine tuned by adjusting the mole ratios of OVS and benzene. They feature both micro- and mesopores (HPP-1 and HPP-2) to almost mesopores (HPP-3 and HPP-4) in the networks. The ratios of micropore volume to total pore volume for HPP-1 to HPP-4 were 0.58, 0.42, 0.10, and 0.11, respectively. These materials exhibit comparable surface area and high thermal stability in N₂ atmosphere. The gas sorption applications reveal that HPP-3 possesses H₂ uptake of 3.47 mmol g⁻¹ (0.70 wt%) at 77 K and 760 mmHg and CO₂ uptake of 0.62 mmol g⁻¹ (2.73 wt%) at 298 K and 760 mmHg. These results indicate these materials are promising candidates for storing H₂ and CO₂. In addition, HPP-4 has been successfully postfunctionalized with 3-mercaptopropionic acid via thiol–ene “click” reaction.

Introduction

Much effort has been devoted to the synthesis of novel porous polymers^[1] because these materials have extensive potential applications, such as gas storage,^[2] gas separation,^[3] heterogeneous catalysis^[4] and drug delivery.^[5] Porous polymers can be easily and effectively prepared via direct synthesis methodology by selecting specific polymerization reactions. This strategy has characteristic advantages, such as high utilization efficiency of the starting materials and easy formation of micropores.^[6] The selection of building blocks and polymerization reactions is the key goal in this strategy. The building blocks should possess geometric restrictions to achieve porous frameworks with adequate stability. The advantageous functionalities can be introduced into the frameworks by using building blocks bearing desired functional groups. The reactions should ensure high efficiency and yields to link the building blocks.

Polyhedral oligomeric silsesquioxane (POSS), with a typical formula of R₈Si₈O₁₂, is a novel kind of organic–inorganic hybrid materials.^[7] This molecule and its derivatives possess well-defined, three-dimensional, and nanometer-sized structures. They are rigid and highly functional, which make them exceptionally robust with respect to heat and water.^[8] Moreover, one feature of cubic POSS

molecules is the similarity to the secondary building units of zeolites; their structures are equal to the 4,4' unit in the LTA and ACO topologies of zeolites. These features indicate their potential as ideal building blocks in preparing micro/mesoporous materials.^[9] Meanwhile, bearing specific functional groups in the POSS moieties is possible to control over the functionalities. A large number of micro/mesoporous polymers have been prepared by using POSS derivatives as building blocks.^[10] A typical methodology to generate porous networks derived from POSS-based building blocks is the direct synthesis procedure. The reactions selected in this procedure involve hydrosilation,^[9,10e] Sonogashira coupling reaction,^[10d] Yamamoto coupling reaction,^[11] and so on. Zhang *et al.* constructed porous polymers with apparent Brunauer–Emmett–Teller (BET) surface areas (*S*_{BET}) of 380 m² g⁻¹ to 530 m² g⁻¹ by using octavinylsilsesquioxane (OVS) and octahydridosilsesquioxane as building blocks via hydrosilation reaction.^[10e] Palladium-catalyzed Heck reaction has been employed to fabricate POSS-based porous polymers with *S*_{BET} of up to 875 m² g⁻¹.^[12] However, these reactions generally require noble metal catalysts, and the preparation of functional POSS derivatives is complicated and typically entails multiple procedures. Therefore, developing new strategies suitable for simple and relatively low-cost synthesis of porous polymers is necessary.

Friedel–Crafts alkylation reaction has become an important method for assembling molecules^[13] and polymers^[14] because this reaction requires relatively mild conditions without any expensive catalyst, but achieves high efficiency. Reports have demonstrated that constructing porous polymers via Friedel–Crafts reaction is versatile and flexible and allows economical and large-scale production of porous materials.^[15] Tan *et al.* reported hypercrosslinked aromatic heterocyclic-based microporous polymers that exhibit highly selective CO₂ capture via Friedel–Crafts reaction.^[15b] These materials are composed of pure organic components, which may result in low thermal stability and mechanical strength. However, the introduction of inorganic–organic hybrid moieties such as POSS-based units could overcome these drawbacks. Chaikkittisilp *et al.* reported hybrid porous nanocomposites with ultrahigh surface area ($S_{\text{BET}} = 2500 \text{ m}^2 \text{ g}^{-1}$) by using benzyl chloride-terminated cubic POSS derivative via Friedel–Crafts reaction.^[10a] However, the synthesis method of the selected POSS-based monomer is uneconomical.

In this paper, we report a simple strategy for constructing POSS-based hybrid porous polymers (HPPs) using OVS and benzene as building blocks via Friedel–Crafts reaction. The selected POSS derivative OVS is easy to obtain and has been extensively utilized to fabricate nanohybrid materials.^[16] The resulting materials, HPP-1 to HPP-4, possess high surface areas and thermal stability. Their porosities can be tuned by changing the mole ratio of benzene to OVS. To further investigate their applications, gas storages, including H₂ and CO₂ are conducted. Finally, postfunctionalization is explored via thiol–ene “click” reaction.

Experimental Section

Materials

Unless otherwise noted, all reagents were obtained from commercial suppliers and used without further purification. OVS was prepared according to previous reports.^[17] Benzene was distilled over CaH₂ at reflux for 12h and stored with 4 Å molecule sieves prior to use. CS₂ was purified using atmospheric distillation methods and stored with 4 Å molecule sieves prior to use.

Characterization

Fourier-transformed infrared (FT-IR) spectra were characterized by Bruker TENSOR27 infrared spectrophotometer from 4000 cm⁻¹ to 400 cm⁻¹ at a resolution of 4 cm⁻¹. The sample was prepared using conventional KBr disk method. Solid-state ¹³C CP/MAS NMR and ²⁹Si MAS NMR spectra were performed on Bruker AVANCE-500 NMR spectrometer operating at a magnetic field strength of 9.4 T. The resonance frequencies at this field strength were 125 and 99 MHz for ¹³C NMR and ²⁹Si NMR, respectively. A chemagnetics of 5 mm triple-resonance MAS probe was used to acquire ¹³C and ²⁹Si NMR spectra. ²⁹Si MAS NMR spectra with high power proton decoupling were recorded with $\pi/2$ pulse length of 5 μs , recycle delay of 120 s, and spinning rate of 5

kHz. Elemental analyses were conducted using Elementarvario EL III elemental analyzer.

Field-emission scanning electron microscopy (FE-SEM) experiments were characterized by a HITACHI S4800 spectrometer. High-resolution transmission electron microscopy (HRTEM) experiments were recorded using a JEM 2100 electron microscope (JEOL, Japan) with an acceleration voltage of 200 kV.

Thermal gravimetric analysis (TGA) was performed on a Mettler Toledo model SDTA 854 TGA system under N₂ atmosphere at a heating rate of 10 °C min⁻¹ from room temperature to 800 °C. Powder X-ray diffraction (PXRD) images were collected on a Rigaku D/MAX 2550 diffractometer under Cu-K α radiation, 40 kV, and 200 mA with a scanning rate of 10° min⁻¹.

N₂ sorption isotherm measurements were characterized by a Micromeritics surface area and pore size analyzer. Before measurement, the samples were degassed for 12 h at 160 °C. A sample of ca. 100 mg and a UHP-grade N₂ (99.999%) gas source were adopted in the N₂ sorption measurements at 77 K and collected on a Quantachrome Quadrasorb apparatus. S_{BET} was confirmed over a P/P_0 range from 0.01 to 0.20. Nonlocal density functional theory (NL-DFT) pore size distributions (PSDs) were determined by C/slit-cylindrical pore mode of the Quadrawin software. CO₂ isotherms were measured at 298 K at 0.0 bar to 1.0 bar. H₂ adsorption capacity was measured at 77 K at 0.0 bar to 1.0 bar. Before measurement, the samples were degassed at 150 °C under vacuum for about 15 h.

Synthesis of HPPs

OVS (1 g, 1.58 mmol), anhydrous AlCl₃ (0.2 g, 1.5 mmol), stoichiometric benzene (12.64 mmol for HPP-1; 6.32 mmol for HPP-2; 4.21 mmol for HPP-3; 3.16 mmol for HPP-4), and CS₂ (10 mL) were charged in an oven-dried flask. The resulting mixture was vigorously stirred at room temperature for 0.5 h and under reflux for 24 h. After the mixture was cooled to room temperature, the mixture was filtered and washed with anhydrous ethanol, acetone, water, and tetrahydrofuran (THF). The products were obtained under the Soxhlet extractor with dichloromethane for 48 h, and dried in vacuo at 60 °C for 48 h.

HPP-1 was afforded as a slightly pink powder (2.0 g). Yield: 92%. Elemental analysis calc. (wt%) for C₅₆H₆₄Si₈O₁₂: C 61.11, H 5.77; Found C 59.68, H 5.37.

HPP-2 was afforded as a slightly pink powder (1.5 g). Yield: 100%. Elemental analysis calc. (wt%) for C₄₀H₄₈Si₈O₁₂: C 50.81, H 5.12; Found C 48.34, H 5.02.

HPP-3 was afforded as a slightly pink powder (1.3 g). Yield: 100%. Elemental analysis calc. (wt%) for C₃₂H₄₀Si₈O₁₂: C 45.68, H 4.79; Found C 44.42, H 5.28.

HPP-4 was afforded as a slightly pink powder (1.2 g). Yield: 100%. Elemental analysis calc. (wt%) for C₂₈H₃₆Si₈O₁₂: C 42.61, H 4.60; Found C 41.57, H 5.24.

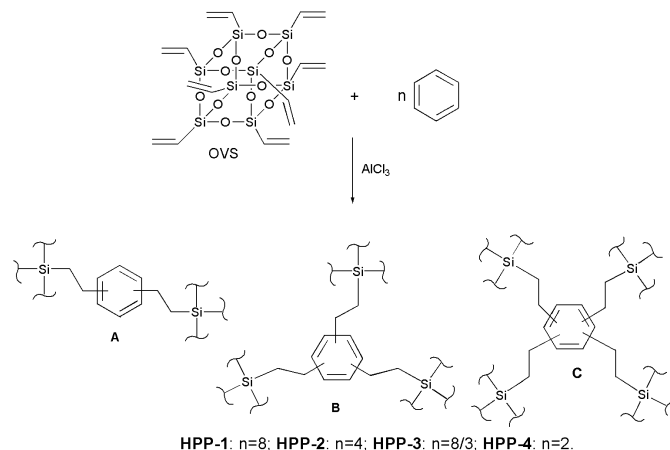
Postfunctionalization of HPP-4 via thiol–ene “click” reaction^[18]

HPP-4 (0.10 g) was suspended in a solution containing 3-mercaptopropionic acid (1.0 g, 9.42 mmol) in THF (10 ml). The resulting mixture was excessively stirred for 1 h at room temperature and irradiated by high-intensity ultraviolet (365

nm) with a spectroline Model SB-100P/FA lamp for 10 min. The product was filtrated and washed with an excessive amount of deionized water and ethanol three times. The sample was purified under a Soxhlet extractor with dichloromethane for 48 h and dried in vacuo at 60 °C for 24 h.

Results and discussion

As shown in Scheme 1, the HPPs were prepared by using OVS to react with stoichiometric benzene via Friedel–Crafts alkylation reaction with AlCl_3 as catalyst. The resulting products were insoluble in all common organic solvents because of their highly cross-linking structures. The polymers were characterized by FT-IR spectroscopy (Figure S1 in the Supporting Information). Compared with the FT-IR pattern of OVS, the intensities of the peaks at 3076, 1603, 1410, and 1275 cm^{-1} , which are associated with the vinyl groups in HPP-1 to HPP-4 decreased at different levels. These results indicate that the polymerization reaction occurred in different degrees. The intensity of the peak at 1603 cm^{-1} increased with decreasing amount of benzene. The phenomena suggest that the unreacted vinyl content in the resulting materials increased with the decreasing amount of benzene. The strong peak at $\sim 1109 \text{ cm}^{-1}$ was attributed to typical Si–O–Si stretching vibrations, proving the presence of cubic silsesquioxane cages.^[10,12]



Scheme 1. Synthetic routes of HPP-1 to HPP-4. Some possible fragments A, B and C in the networks are shown as examples.

To confirm the structures of the polymers, solid-state ^{13}C CP/MAS NMR and ^{29}Si MAS NMR spectroscopy were also performed. Considering the similar chemical structures of HPP-1 to HPP-4, we selected HPP-4 as an example. Figure 1(a) shows the ^{13}C CP/MAS NMR spectrum of HPP-4. The resonance peaks in the range of 142.7 ppm to 127.9 ppm were ascribed to the carbon atoms derived from the bridging phenyl units and the unreacted Si–CH=CH₂. The signals at $\delta = 28.9$ and 13.8 ppm can be assigned to the two carbon atoms at the linker units of Si–CH₂–CH₂– formed after the Friedel–Crafts reaction,^[19] confirming the success of the cross-linking reaction.

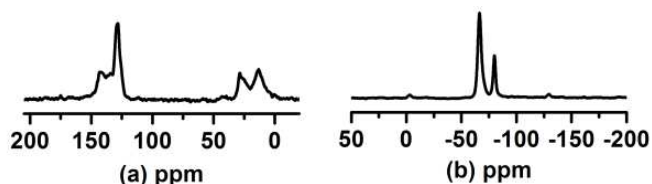


Figure 1. (a) Solid-state ^{13}C MAS NMR spectrum of HPP-4. (b) Solid-state ^{29}Si MAS NMR spectrum of HPP-4.

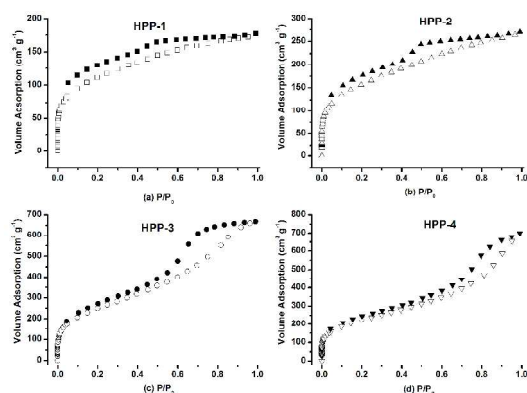
Figure 1(b) shows the solid-state ^{29}Si MAS NMR spectrum of HPP-4. Compared with the solid-state ^{29}Si MAS NMR spectra of OVS,^[10b] the signals at -67 and -80 ppm can be ascribed to the silicon atoms of T₃ units (T_n: $\text{CSi}(\text{OSi})_n(\text{OH})_{3-n}$) from the Si–CH₂–CH₂– units formed after Friedel–Crafts reaction and the unreacted Si–CH=CH₂ units, respectively. In comparison to other POSS-based porous polymers,^[10e,12] no T₁ or T₂ unit is observed, suggesting that no POSS cage in the framework collapsed during synthesis. In previous reports, a few POSS cages collapsed through several polymerization reactions such as Sonogashira coupling,^[10d] Heck coupling,^[12] as well as Friedel–Crafts reactions.^[10a] In the current study, the intact POSS cages could be ascribed to three aspects. First, special care was taken to minimize contamination with water and oxygen. No amine (such as triethylamine used in Sonogashira and Heck coupling) was added as base which could cleave the siloxane bonds. Second, unlike other synthesis via Friedel–Crafts reactions, no HCl, which could also break POSS cages, was produced in this system. The third aspect is the flexible linking units, i.e., –CH₂–CH₂–Ph–CH₂–CH₂–. Previous reports suggest that POSS cages would be distorted to reduce the structural constraints or stresses of the resulting networks when POSS cages are connected by rigid linking units, such as the arylene ethynylene groups and arylene ethynylene groups formed by Heck and Sonogashira coupling, respectively.^[12b,10d] The distortion can result in the destruction of POSS cages. In the present study, the relatively flexible linking connections can decrease the structural constraints and thus retain the intact POSS cages in the framework.

The porosity parameters of the polymers were characterized by N₂ adsorption–desorption analysis at 77 K (Figure 2). All of the samples showed sharp uptake at low relative pressures and gradually increasing uptake at higher relative pressures with hysteresis, indicating that these materials contained both micro- and mesopores.^[10] The hysteresis in HPP-3 and HPP-4 was more evident than that in HPP-1 and HPP-2, implying the higher ratio of mesopore volume over total pore volume in HPP-3 and HPP-4. The porosity data of these polymers are shown in Table 1. S_{BET} for HPP-1 to HPP-4 were calculated as 400, 565, 904, and 802 $\text{m}^2 \text{g}^{-1}$, respectively. The micropore surface areas were calculated as 253, 297, 189, and 220 $\text{m}^2 \text{g}^{-1}$, respectively, using the t -plot method. The surface areas of the hybrid polymers first increased and then decreased with the increase of the mole ratio of OVS to benzene, and approached a maximum S_{BET} of 904 $\text{m}^2 \text{g}^{-1}$ when the ratio was 3:8 (HPP-3).

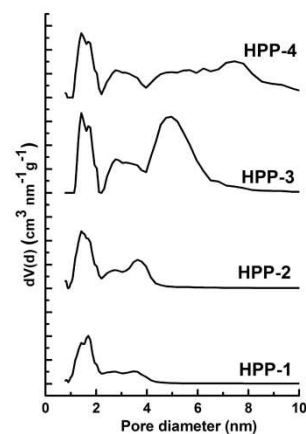
Table 1. Porosity data of HPP-1 to HPP-4.

Sample	Mole ratio of OVS to benzene	$S_{\text{BET}}^{[a]}/\text{m}^2\text{g}^{-1}$	$S_{\text{micro}}^{[b]}/\text{m}^2\text{g}^{-1}$	$V_{\text{total}}^{[c]}/\text{cm}^3\text{g}^{-1}$	$V_{\text{micro}}^{[d]}/\text{cm}^3\text{g}^{-1}$	$V_{\text{micro}}/V_{\text{total}}$
HPP-1	1:8	400	253	0.24	0.14	0.58
HPP-2	2:8	565	297	0.38	0.16	0.42
HPP-3	3:8	904	189	0.96	0.10	0.10
HPP-4	4:8	802	220	0.99	0.11	0.11

[a] Surface area calculated from N_2 adsorption isotherm using BET method; [b] Microporous surface area calculated from N_2 adsorption isotherm using t -plot method; [c] Total pore volume calculated at $P/P_0 = 0.99$; [d] Micropore volume derived using t -plot method based on the Halsey thickness equation.

**Figure 2.** N_2 sorption isotherms of HPP-1 to HPP-4.

PSDs were calculated from the NL-DFT. The results agree with the patterns of N_2 isotherms and suggest that micro- and mesopores coexisted in all porous polymers. As shown in Fig. 3, HPP-1 and HPP-2 exhibited similar PSD to uniform micropores with an average diameter centered at about 1.5 nm and a broad distribution of mesopores with predominant diameters at 2.5 and 3.5 nm. HPP-3 possessed uniform micropores with an average diameter centered at 1.4 nm and a broader distribution of mesopores at 2.8 and 4.8 nm compared with HPP-1 and HPP-2. HPP-4 showed uniform micropores with an average diameter centered at 1.4 nm and a much broader distribution of mesopores from 2 nm to 10 nm compared with HPP-3. The total pore volumes (V_{total}) were 0.24, 0.38, 0.96, and 0.99 cm^3g^{-1} for HPP-1 to HPP-4, respectively. The contribution of microporosity to the networks can be calculated from the micropore volume (V_{micro}) over V_{total} . The ratios of $V_{\text{micro}}/V_{\text{total}}$ for HPP-1 to HPP-4 were 0.58, 0.42, 0.10, and 0.11, respectively. The results confirmed that HPP-3 and HPP-4 possessed more mesopores than HPP-1 and HPP-2, agreeing with the patterns of N_2 isotherms.

**Figure 3.** NL-DFT PSDs HPP-1 to HPP-4.

Based on these results, a remarkable feature of these materials is that their porosities can be fine tuned by adjusting the mole ratio of OVS to benzene. Compared with HPP-1 and HPP-2, a nearly twofold increase for the surface area and threefold increase for the pore volume were found in HPP-3 and HPP-4. By contrast, the ratios of $V_{\text{micro}}/V_{\text{total}}$ decreased and PSD became broad in the mesopore region (2 nm to 10 nm). HPP-3 and HPP-4 can be considered as mesoporous materials because of their low ratios of $V_{\text{micro}}/V_{\text{total}}$. The tunable porosity can be correlated with the multi-reaction sites of benzene and different cross-linking densities. When the vinyl groups reacted with benzene, the number and position of the reaction sites on the phenyl units were adjustable and varied by changing the amount of benzene.^[20] When an excessive amount of benzene was added in the reaction system, a small molecular compound, i.e., octaphenethylsilsesquioxane was formed because benzene units mainly provided one reaction site to link the vinyl groups.^[19] With the decreasing amount of benzene, the benzene unit can be linked by two, three, or four vinyl groups and cross-linking networks were afforded. The possible fragments (**A**, **B**, and **C**) in the networks are shown in Scheme 1. Owing to the steric hindrance, we anticipate that the fragments that phenyl units linked by more than four vinyl groups were very few. Evidently, different fragments could result in different cross-linking densities that affect the surface areas and PSD.

For HPP-1, the mole ratio of OVS to benzene was 1:8 and fragment **A** mainly existed in the networks, resulting in relatively uniform cross-linking density and PSD. For HPP-2, fragment **B** may be formed. PSD became broader compared with HPP-1. With the decreasing amount of benzene, the generation probabilities of fragments **B** and **C** could be enhanced, which may result in inhomogeneous cross-linking density and produce much broader PSD for HPP-3 and HPP-4 than HPP-1 and HPP-2. Higher surface areas and pore volumes were also found for HPP-3 and HPP-4. Fragments **B** and **C** indicated higher cross-linking density than fragment **A**, which could lead to higher surface area and pore volume.^[20] Meanwhile, the increasing local cross-linking density may afford more mesopores; thus, HPP-3 and HPP-4 featured almost mesopores, which was consistent with a previous report.^[10d] Given that fragment **C** possessed larger steric hindrance than fragment **B**, the main fragments in HPP-4 and

HPP-3 may be similar. Thus, more vinyl groups were residual in HPP-4 than in HPP-3, as also proven by FTIR results described above. Therefore, the residual vinyl groups in HPP-4 occupied more free volume than HPP-3, which could lead to lower surface area and pore volume. These results confirm that cross-linking density strongly affected the porosity of the resulting networks.^[20]

The polymers exhibited apparent S_{BET} and pore volumes, which were comparable to those of other POSS-based porous polymers,^[10b,21] conjugated microporous polymers (CMPs),^[22] and metal–organic frameworks (MOFs).^[23] Compared with other OVS-based porous polymers,^[9,10e] these polymers displayed higher S_{BET} , larger pore volumes and broader PSDs. However, these values were still relatively lower than the highest values for other POSS-based porous polymers.^[10a] The results may be ascribed to the short structure length and the weak rigidity of the resulting linker $-\text{CH}_2-\text{CH}_2-\text{Ph}-\text{CH}_2-\text{CH}_2-$. However, this reaction was low-cost and facile to conduct. The selected monomers were easy to obtain and inexpensive. Therefore, we present a facile and low-cost strategy for constructing porous materials with tunable porosity.

To evaluate the thermal stability of the polymers, TGA was performed under N_2 at $10\text{ }^\circ\text{C min}^{-1}$ from room temperature to $800\text{ }^\circ\text{C}$. The first mass loss of OVS (Figure 4) is ascribed to the cleavage of the peripheral vinyl groups; the sharp mass loss near $300\text{ }^\circ\text{C}$ indicates overlapping destructions of the inorganic POSS cages and vinyl groups.^[24] In addition, the residue of OVS in N_2 was very low; hydrogen POSS and some alkyl-substituted POSS (e.g., methyl, ethyl, and isobutyl) also exhibited similar thermal degradation behavior in N_2 . Such behavior is attributed to volatilization, which is the evaporation or sublimation in inert atmosphere; in air, the organic chains undergo oxidation reaction, which leads to cage crosslinking, thereby producing a ceramic silica-like phase.^[25] The resulting hybrid porous materials exhibited good thermal stability. The polymers exhibited high thermal decomposition temperature (T_d at 5 wt%) of approximately $520\text{ }^\circ\text{C}$, which was significantly higher than that of OVS. This characteristic is ascribed to the formation of highly crosslinked networks after the Friedel–Crafts reaction. The initial decomposition can be ascribed to the rupture of organic moieties, including the unreacted vinyl groups and the $\text{Si}-\text{CH}_2-\text{CH}_2-\text{Ph}$ units. The decomposition that occurred at about $540\text{ }^\circ\text{C}$ may be attributed to the fragmentation of the siloxane spacers. These materials were more stable than other POSS-based porous polymers,^[11,12] which could be attributed to the intact POSS cages in the frameworks proven by the solid-state ^{29}Si MAS NMR.

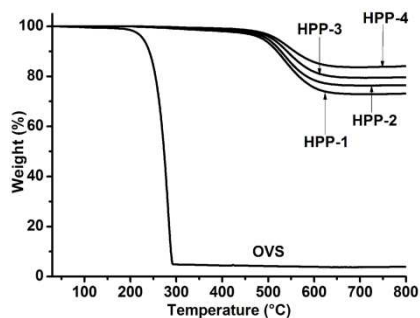


Figure 4. TGA curves of OVS and HPP-1 to HPP-4.

The morphologies of the polymers were investigated by PXRD, FE-SEM and HRTEM. The PXRD results illustrated that OVS was highly crystalline (Figure 5). The polymers were amorphous, and no long-range crystallographic order in their structures was observed. The broad diffraction peaks emerged at $\sim 22^\circ 2\theta$, which were evidently associated with the $\text{Si}-\text{O}-\text{Si}$ linkages.^[26]

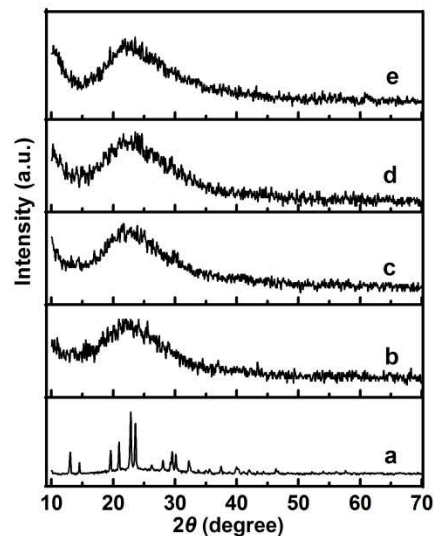


Figure 5. XRD patterns of (a) OVS, (b) HPP-1, (c) HPP-2, (d) HPP-3, and (e) HPP-4.

Figure 6(a) shows the FE-SEM image of HPP-1. The FE-SEM images of other porous hybrids are shown in the supporting information (Figure S2 to S4). All of samples exhibited similar morphologies and irregular shapes, with wide range size distribution ranging from 100 nm to several micrometers, similar to other amorphous porous materials.^[27,28] Figure 6(b) displays the HRTEM image of HPP-1. The HRTEM images of HPP-2, HPP-3, and HPP-4 are provided in the supporting information (Figure S5 to S7). These results indicate that the polymers exhibited the features of amorphous porous materials without long-range ordering. The samples were stable under the electron beam.

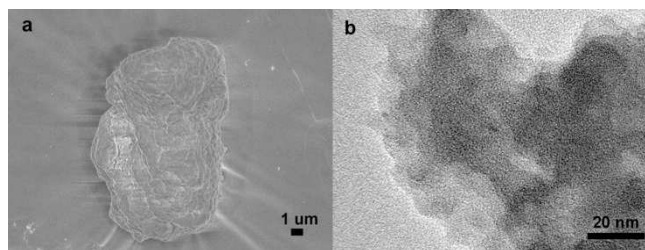


Figure 6. (a) FE-SEM image of HPP-1. (b) HRTEM image of HPP-1.

Gas storage is one of the most promising applications for porous materials.^[29] To evaluate the performances of the polymers in gas storage, particularly in storing H_2 and capturing CO_2 , H_2 and CO_2 sorption experiments at 77 and 298 K were performed using volumetric methods. As the polymers possessed similar chemical structure, we selected HPP-3

because it exhibited the highest S_{BET} . The H_2 storage capacity for HPP-3 was 3.48 mmol g^{-1} (0.70 wt%) at 77 K and 760 mmHg (Figure 7a). The CO_2 uptake for HPP-3 was 0.62 mmol g^{-1} (2.73 wt%) at 298 K and 760 mmHg (Figure 7b). These values were comparable to other microporous polymers with a level of surface areas.^[10d,30] Chaikittisilp *et al.* reported that PSN-1 with S_{BET} of $850 \text{ m}^2 \text{ g}^{-1}$ exhibited H_2 storage uptake of 0.89 wt% at 77 K and 760 Torr;^[10d] PSN-1 was constructed from bromophenylethenyl-terminated POSS and 1,3-diethynylbenzene units via Sonogashira cross-coupling reaction. Dawson *et al.* reported that the CO_2 storage capacity for CMP-1-(CH_3)₂ with S_{BET} of $899 \text{ m}^2 \text{ g}^{-1}$ was 0.94 mmol g^{-1} at 298 K and 1.0 bar; CMP-1-(CH_3)₂ was formed by 1,3,5-triethynylbenzene and 1,4-dibromo-2,5-dimethylbenzene via Sonogashira reaction.^[30b] These results indicate that the polymers could be applied as promising candidates for H_2 and CO_2 capture and storage.

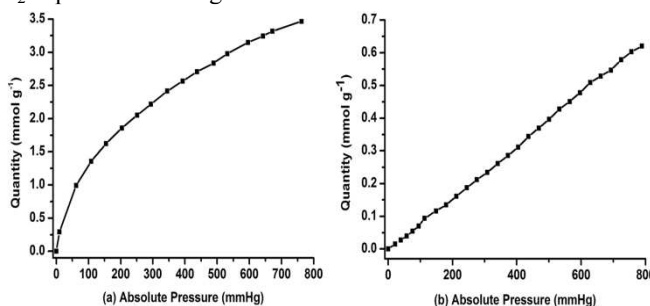


Figure 7. Gas sorption isotherms of HPP-3. (a) H_2 adsorption isotherm at 77 K. (b) CO_2 adsorption isotherm at 298 K.

Postfunctionalization is important to extend the applications of porous materials because their physicochemical properties can be tuned by the selection of functional groups.^[30,31] Among several strategies for postfunctionalization in previous reports,^[16] the thiol-ene “click” reaction is a simple and effective route to modify the framework or surface of porous polymers using residual vinyl groups with thermal or photochemical methods.^[32] Carboxyl-functionalized porous materials have numerous applications, including synthetic ion channels, acidic catalysts, heavy metal ion adsorption and ligands for inorganic/organic species.^[33] The carboxyl groups in the porous structure may also serve as anchoring sites in biomolecule and polypeptide syntheses.^[34] Therefore, 3-mercaptopropyl acid was selected for the reaction with residual vinyl groups in the hybrid porous materials. Considering the similar chemical structure and the vinyl content in HPP-1 to HPP-4, HPP-4 was selected in this study as the sample and postfunctionalized with 3-mercaptopropionic acid through thiol-ene “click” reaction. The resulting hybrid polymer was confirmed by FT-IR spectroscopy (Figure S8 in the Supporting Information). The intensity of the characteristic peak for vinyl groups at 1603 cm^{-1} obviously decreased. New peaks at 3610 and 1720 cm^{-1} , which are respectively associated with hydroxyl and carbonyl groups, appeared in the postfunctionalized product in comparison to those of HPP-4. This result indicates that the 3-mercaptopropionic acid was partially added to HPP-4. To confirm the structure of the resulting material, the solid-state ^{13}C CP/MAS NMR (Figure S9 in the Supporting Information) and ^{29}Si MAS NMR (Figure S10 in the Supporting Information) analyses were also performed. The resonance peak near 175.3 ppm was ascribed to the carboxyl carbon atom ($-\text{COOH}$) from

3-mercaptopropionic acid. The resonance peak near 35.1 ppm was ascribed to the α carbon atom linking the $-\text{COOH}$. The resonance peak near 17.9 ppm was assigned to the β carbon atom in the $\text{Si}-\text{CH}_2-\text{CH}_2-\text{S}-$ formed after the thiol-ene “click” reaction. According to the ^{29}Si MAS NMR of HPP-4 and the postfunctionalized product, the intensity of the peak near -67 ppm obviously decreased, suggesting that the partial transformation of the vinyl groups to the alkyl groups occurred after the thiol-ene “click” reaction.

The porosity property of the postfunctionalized product was also characterized by N_2 adsorption-desorption analysis at 77 K (Figure S11 in the Supporting Information). S_{BET} was $568 \text{ m}^2 \text{ g}^{-1}$, and the micropore surface area was calculated as $60 \text{ m}^2 \text{ g}^{-1}$ using the t -plot method. The pore volume was $0.56 \text{ cm}^3 \text{ g}^{-1}$ calculated at $P/P_0 = 0.99$. The PSD result indicates that the product contained uniform micropores with an average diameter centered at 1.5 nm and a broad distribution of mesopores between 2.3 and 6.4 nm (Figure S12 in the Supporting Information). Compared with HPP-4, the porosity data decreased at different degrees and the pore diameter of the mesopores became uniform and small. The framework with carboxyl groups may enable extensive potential applications, such as catalysis and heavy metal ion adsorption.

Conclusion

Through ingenious design, cubic OVS and benzene were introduced as building blocks to construct HPPs via Friedel-Crafts reaction. The resulting polymers, HPP-1 to HPP-4, were highly porous with both micro- and mesopores. Their porosities can be tuned by changing the mole ratios of OVS to benzene. They showed relatively high surface areas, with S_{BET} ranging from $400 \text{ m}^2 \text{ g}^{-1}$ to $904 \text{ m}^2 \text{ g}^{-1}$ and pore volumes ranging from $0.24 \text{ cm}^3 \text{ g}^{-1}$ to $0.99 \text{ cm}^3 \text{ g}^{-1}$. These materials exhibited comparable surface areas and high thermal stability compared with other POSS-based porous polymers, MOFs, and COFs materials. The gas sorption applications reveal that HPP-4 possessed comparable H_2 uptake of 3.47 mmol g^{-1} (0.70 wt%) at 77 K and 760 mmHg and CO_2 uptake of 0.62 mmol g^{-1} (2.73 wt%) at 298 K and 760 mmHg, indicating its potential in gas storage for H_2 and CO_2 . The postfunctionalized result also indicates HPPs can be easily modified with thiohydraacrylic acid via thiol-ene click reaction.

Acknowledgements

This research was supported by the National Natural Science Foundation of China (21274080 and 21274081) and the Independent Innovation Foundation of Shandong University (IIFSDU).

Notes and references

^aKey Laboratory of Special Functional Aggregated Materials, Ministry of Education, School of Chemistry and Chemical Engineering, Shandong University, Jinan 250100, P. R. China.

^bKey Laboratory of Fine Chemicals in Universities of Shandong, Shandong Polytechnic University, Jinan 250353, P. R. China.

Fax: +86-531-88564464; E-mail: (H. Liu) liuhongzhi@sdu.edu.cn.

Electronic Supplementary Information (ESI) available: FT-IR spectra of the hybrid porous polymers, partial FE-SEM images, and HRTEM images of the HPPs, ^{13}C CP/MAS NMR, and ^{29}Si MAS NMR of HPP-4 postfunctionalized with 3-mercaptopropionic acid, as well as and the porosity of HPP-4 modified with 3-mercaptopropionic acid are available free of charge via the Internet. See DOI: 10.1039/b000000x/

1. a) Q. Zhang, S. Zhang and S. Li, *Macromolecules*, 2012, **45**, 2981; b) X. S. Zhao, *J. Mater. Chem.*, 2006, **16**, 623; c) X. Liang, S. M. George, A. W. Weimer, N. Li, J. H. Blackson, J. D. Harris and P. Li, *Chem. Mater.*, 2007, **19**, 5388.
2. a) E. Masika and R. Mokaya, *J. Phys. Chem. C*, 2012, **116**, 25734; b) Y. Zhao, L. Zhao, K. Yao, Y. Yang, Q. Zhang and Y. Han, *J. Mater. Chem.*, 2012, **22**, 19726; c) S. Ding and W. Wang, *Chem. Soc. Rev.*, 2013, **42**, 548; d) Z. Xiang, X. Zhou, C. Zhou, S. Zhong, X. He, C. Qin and D. Cao, *J. Mater. Chem.*, 2012, **22**, 22663; e) F. Vilela, K. Zhang and M. Antonietti, *Energy Environ. Sci.*, 2012, **5**, 7819.
3. a) Z. Chang, D. Zhang, Q. Chen and X. Bu, *Phys. Chem. Chem. Phys.*, 2013, **15**, 5430; b) C. E. Wilmer, O. K. Farha, Y. S. Bae, J. T. Hupp and R. Q. Snurr, *Energy Environ. Sci.*, 2012, **5**, 9849; c) R. Eguchi, S. Uchida and N. Mizuno, *Angew. Chem., Int. Ed.*, 2012, **51**, 1635.
4. a) M. E. Davis, *Nature*, 2002, **417**, 813. b) N. B. McKeown and P. M. Budd, *Chem. Soc. Rev.*, 2006, **35**, 675; c) Y. Wan, H. Wang, Q. Zhao, M. Klingstedt, O. Terasaki and D. Zhao, *J. Am. Chem. Soc.*, 2009, **131**, 4541.
5. a) S. Marchesan and M. Prato, *Med. Chem. Lett.*, 2013, **4**, 147; b) E. Cassette, M. Helle, L. Bezdetsnaya, F. Marchal, B. Dubertret and T. Pons, *Adv. Drug Deliv. Rev.*, 2013, **65**, 719.
6. D. Wu, F. Xu, B. Sun, R. Fu, H. He and K. Matyjaszewski, *Chem. Rev.*, 2012, **112**, 3959.
7. S. W. Kuo, Chang, F. C. *Prog. Polym. Sci.*, 2011, **36**, 1649.
8. a) Y. Ni, S. X. Zheng and K. M. Nie, *Polymer*, 2004, **45**, 5557; b) K. Tanaka and Y. Chujo, *J. Mater. Chem.*, 2012, **22**, 1733; c) R. M. Laine, and M. F. Roll, *Macromolecules*, 2011, **44**, 1073; d) D. B. Cordes, P. D. Lickiss and F. Rataboul, *Chem. Rev.*, 2010, **110**, 2081.
9. J. J. Morrison, C. J. Love, B. W. Manson, I. J. Shannon and R. E. Morris, *J. Mater. Chem.*, 2002, **12**, 3208.
10. a) W. Chaikittisilp, M. Kubo, T. Moteki, A. Sugawara-Narutaki, A. Shimojima and T. Okubo, *J. Am. Chem. Soc.*, 2011, **133**, 13832; b) I. Nischang, O. Brüggemann and I. Teasdale, *Angew. Chem., Int. Ed.*, 2011, **50**, 4592; c) Y. Peng, T. Ben, J. Xu, M. Xue and S. Qiu, *Dalton Trans.*, 2011, **40**, 2720; d) W. Chaikittisilp, A. Sugawara, A. Shimojima, and T. Okubo, *Chem. Eur. J.*, 2010, **16**, 6006; e) C. Zhang, F. Babonneau, C. Bonhomme, R. M. Laine, C. L. Soles, H. A. Hristov and A. F. Yee, *J. Am. Chem. Soc.*, 1998, **120**, 8380; f) Y. Wada, K. Iyoki, A. Sugawara-Narutaki, T. Okubo and A. Shimojima, *Chem. Eur. J.*, 2013, **18**, 1700; g) F. Alves, P. Scholder and I. Nischang, *ACS Appl. Mater. Interfaces*, 2013, **5**, 2517; h) M. Wu, R. Wu, R. Li, H. Qin, J. Dong, Z. Zhang and H. Zou, *Anal. Chem.*, 2010, **82**, 5447.
11. W. Chaikittisilp, A. Sugawara, A. Shimojima and T. Okubo, *Chem. Mater.*, 2010, **22**, 4841.
12. a) D. Wang, L. Xue, L. Li, B. Deng, S. Feng, H. Liu and X. Zhao, *Macromol. Rapid Commun.*, 2013, **34**, 861; b) D. Wang, W. Yang, L. Li, X. Zhao, S. Feng and H. Liu, *J. Mater. Chem. A*, 2013, **1**, 13549.
13. B. Gao, F. Li and J. Men, *Polymer*, 2012, **53**, 4709.
14. a) S. Ishikawa, M. Ito and M. Okamoto, *Polymer*, 1996, **37**, 3763; b) R. Dawson, A. I. Cooper and D. J. Adams, *Prog. Polym. Sci.*, 2012, **37**, 530.
15. a) Y. Luo, B. Li, W. Wang, K. Wu and B. Tan, *Adv. Mater.*, 2012, **24**, 5703; b) B. Li, R. Gong, W. Wang, X. Huang, W. Zhang, H. Li, C. Hu and B. Tan, *Macromolecules*, 2011, **44**, 2410; c) R. Dawson, L. A. Stevens, T. C. Drage, C. E. Snape, M. W. Smith, D. J. Adams and A. I. Cooper, *J. Am. Chem. Soc.*, 2012, **134**, 10741.
16. G. Cheng, N. R. Vautravers, R. E. Morris and D. J. Cole-Hamilton, *Org. Biomol. Chem.*, 2008, **6**, 4662.
17. D. Chen, S. Yi, W. Wu, Y. Zhong, J. Liao, C. Huang and W. Shi, *Polymer*, 2010, **51**, 3867.
18. a) A. K. Tucker-Schwartz, R. A. Farrell and R. L. Garrell, *J. Am. Chem. Soc.*, 2011, **133**, 11026; b) C. E. Hoyle and C. N. Bowman, *Angew. Chem., Int. Ed.*, 2010, **49**, 1540; c) K. Shanmuganathan, R. K. Sankhagowit, P. Iyer and C. J. Ellison, *Chem. Mater.*, 2011, **23**, 4726.
19. E. O. Dare, G. A. Olatunji, D. S. Ogunniyi and A. A. Lasisi, *Polish J. Chem.*, 2005, **79**, 109.
20. a) J. Weber and L. Bergström, *Macromolecules*, 2009, **42**, 8234; b) Y. Kim, K. Koh, M. F. Roll, R. M. Laine and A. J. Matzger, *Macromolecules*, 2010, **43**, 6995; c) Q. Liu, Y. Li, S. Shen and S. Zhou, *Mater. Chem. Phys.*, 2011, **125**, 315.
21. Y. Qin, H. Ren, F. Zhu, L. Zhang, C. Shang, Z. Wei and M. Luo, *Eur. Polym. J.*, 2011, **47**, 853.
22. J.-X. Jiang, F. Su, H. Niu, C. D. Wood, N. L. Campbell, Y. Z. Khimyak and A. I. Cooper, *Chem. Commun.*, 2008, 486.
23. a) M. Park, D. Moon, J. W. Yoon, J.-S. Chang and M. S. Lah, *Chem. Commun.*, 2009, 2026; b) S. Xiang, W. Zhou, Z. Zhang, M. A. Green, Y. Liu and B. Chen, *Angew. Chem., Int. Ed.*, 2010, **49**, 4615.
24. a) D. Neumann, M. Fisher, L. Tran, and J. G. Matison, *J. Am. Chem. Soc.*, 2002, **124**, 13998; b) H. Liu, S. Kondo, N. Takeda and M. Unno, *J. Am. Chem. Soc.*, 2008, **130**, 10074.
25. A. Fina, D. Tabuani, F. Carniato, A. Frache, E. Boccaleri and G. Camino, *Thermochim. Acta*, 2006, **440**, 36.
26. D. Yang, W. Zhang, R. Yao and B. Jiang, *Polym. Degrad. Stab.*, 2013, **97**, 109.
27. R. Dawson, A. Laybourn, Y. Z. Khimyak, D. J. Adams and A. I. Cooper, *Macromolecules*, 2010, **43**, 8524.
28. a) J. Weber and A. Thomas, *J. Am. Chem. Soc.*, 2008, **130**, 6334; b) J.-X. Jiang, F. Su, A. Trewin, C. D. Wood, N. L. Campbell, H. Niu, C. Dickinson, A. Y. Ganin, M. J. Rosseinsky, Y. Z. Khimyak and A. I. Cooper, *Angew. Chem., Int. Ed.*, 2007, **46**, 8574.
29. F. Vilela, K. Zhang and M. Antonietti, *Energy Environ. Sci.*, 2012, **5**, 7819.
30. a) R. Dawson, A. Laybourn, R. Clowes, Y. Z. Khimyak, D. J. Adams and A. I. Cooper, *Macromolecules*, 2009, **42**, 8809; b) R. Dawson, D. J. Adams and A. I. Cooper, *Chem. Sci.*, 2011, **2**, 1173.
31. H. Lim, M. C. Cha and J. Y. Chang, *Polym. Chem.*, 2012, **3**, 868.
32. a) A. B. Lowe, *Polym. Chem.*, 2010, **1**, 17; b) C. E. Hoyle and C. N. Bowman, *Angew. Chem., Int. Ed.*, 2010, **122**, 1584.
33. a) L. Han, Y. Sakamoto, O. Terasaki, Y. Li and S. Che, *J. Mater. Chem.*, 2007, **17**, 1216; b) L. Han, O. Terasaki and S. Che, *J. Mater. Chem.*, 2011, **21**, 11033.
34. N. Liu, R. A. Assink and C. J. Brinker, *Chem. Commun.*, 2003, 370.